Thermal Science and Engineering Progress 41 (2023) 101815

Contents lists available at ScienceDirect

Thermal Science and Engineering Progress

journal homepage: www.sciencedirect.com/journal/thermal-science-and-engineering-progress

Effects of thermal radiation and variable density of nanofluid heat transfer along a stretching sheet by using Keller Box approach under magnetic field

Fehmi Gamaoun [a], Zia Ullah [b,*], N. Ameer Ahammad [c], Bandar M. Fadhl [d], Basim M. Makhdoum [e], Aamir Abbas Khan [f]

[a] Department of Mechanical Engineering, College of Engineering, King Khalid University, Abha 61421, Saudi Arabia
[b] Department of Mathematics and Statistics, The University of Lahore, Sargodha-Campus, Sargodha 40100, Pakistan
[c] Department of Mathematics, Faculty of Science, University of Tabuk, P.O.Box 741, Tabuk 71491, Saudi Arabia
[d] Mechanical Engineering Department, College of Engineering and Islamic Architecture, Umm Al-Qura University, P.O.Box 5555, Makkah 21955, Saudi Arabia
[e] Mechanical Engineering Department, College of Engineering and Islamic Architecture, Umm Al-Qura University, P.O.Box 5555, Makkah 21955, Saudi Arabia
[f] Department of Mathematics, University of Sargodha, Sargodha 40100, Pakistan

ARTICLE INFO

Keywords:
Variable density
Thermal radiation
Nanofluid
Keller box method
Magnetohydrodynamics
Heat transfer
Thermophoresis
Stretching sheet
Mass transfer

ABSTRACT

Most of research has been discovered with lower temperature differential and constant density between the ambient fluid and the surface. The density is assumed as exponential function of temperature due to larger temperature difference with radiation. The magnetohydrodynamics (MHD) acts like a coating material to protect technological devices from excessive heating. Main focus of this mechanism is the variable density, MHD and radiation effects on heat and mass characteristics of nanofluid across stretching sheet with thermophoresis and Brownian motion to reduce excessive heating in high temperature systems. This is first temperature-dependent density problem of nanofluid across the stretching surface. The coupled (PDEs) partial differential equations of the present nanofluid mechanism are changed in nonlinear coupled ordinary differential equations (ODEs) with defined stream functions and similarity variables for smooth algorithm and integration. The changed ODEs are again converted in similar form for numerical outcomes by applying Keller Box approach. The numerical outcomes are deduced in graphs and tabular form with the help of MATLAB program. In this phenomenon, the velocity, temperature, and concentration profile along with their slopes has been plotted for various parameters for current issue. The range of parameters has selected according as Prandtl number $0.07 \leq Pr \leq 70.0$, buoyancy parameter $0 < \xi < \infty$ and the choice of magnetic force parameter set the effects of magnetic diffusion and magnetic energy respectively. The novelty of the current work is to compute radiation, MHD and temperature dependent density effects along the stretching sheet due to high temperature difference between the surface and ambient fluid. By the encountering the radiation fluid becomes optically dense gray fluids. So, the thermal radiation is just used as a supporting agent for heat transfer assessment due to exponentially temperature dependent density.

1. Introduction

The heat, mass, and momentum transfer in the laminar MHD boundary layer nanofluid flow over a stretching sheet is very important in theoretical and practical point of view in metallurgy and polymer technology, nanotechnologies, micro-technologies and nonmaterial. This type of flows appears in various engineering applications such as polymer extrusion, continuous casting, glass fiber and paper production, food manufacturing, stretching of plastic films and several other processes. In recent years, the nanofluids in the presence of a magnetic field find increasing applications in many areas such as chemical engineering, electromagnetic propulsion, nuclear reactors, etc. Nanotechnology plays an important role in many electronic devices, vehicles, space craft, defense, biomedical science, solar water heating, rolling sheet drawn from a die, cooling and/or drying of paper and textile, manufacturing of polymeric sheets, sheet glass, crystalline materials and cooling applications, etc. The cooling of a sizable metallic plate across a stretching surface presents a significant problem in a number of engineering processes, including extrusion, melt-spinning, micro chips, micro-machines, hot rolling, wire drawing, the production of fiber, and the production of plastic/rubber sheets. The simultaneous effects of heat transfer and

* Corresponding author.
E-mail address: ziakhan.uos.72@gmail.com (Z. Ullah).

https://doi.org/10.1016/j.tsep.2023.101815
Received 27 January 2023; Received in revised form 23 March 2023; Accepted 26 March 2023
Available online 30 March 2023

Nomenclature

a	Constant
C	Nanoparticle volume fraction
C_w	Nanoparticle volume fraction at surface
C_∞	Ambient nanoparticle volume fraction
D_B	Brownian diffusion coefficient
D_T	Thermophoretic diffusion coefficient
$f(\eta)$	Dimensionless stream function
κ	Thermal conductivity
Le	Lewis number
N_b	Brownian motion parameter
N_t	Thermophoresis parameter
Nu	Nusselt number
Pr	Prandtl number
p	Pressure
q_m	Wall mass flux
q_w	Wall heat flux
Re_x	Local Reynolds number
Sh_x	Local Sherwood number
T	Fluid temperature
T_w	Temperature at the stretching surface
R_d	Radiation parameter
T_∞	Ambient temperature
u, v	Velocity components along x- and y-axes
u_w	Velocity of the stretching sheet
x, y	Cartesian coordinates

Greek symbols

α	Thermal diffusivity
$\phi(\eta)$	Rescaled nanoparticle volume fraction
η	Similarity variable
$\theta(\eta)$	Dimensionless temperature
ν	Kinematic viscosity of the fluid
ρ_f	Fluid density
ρ_p	Nanoparticle mass density
$(\rho c)_f$	Heat capacity of the fluid
$(\rho c)_p$	Effective heat capacity of the nanoparticle material
τ	Ratio of heat capacity of nanoparticle and fluid
ψ	Stream function
λ	Buoyancy parameter
ξ	Magnetic force parameter
n	Density parameter
σ	Stephen Boltzmann constant
κ^*	Absorption constant

magnetohydrodynamic (MHD) are useful in order to achieve the final product of desire characteristics. Such considerations are very important especially in the metallurgical processes including the cooling of continuous strips and filaments drawn through a quiescent fluid and purification of molten metal from nonmetallic inclusions. In the manufacturing process, the production of polymer sheets and filaments are more important factors. This kind of flow is used in many engineering processes, including plastic film stretching, continuous casting, paper production, food manufacturing, and the extrusion of polymers. It is helpful to influence the combined effects of heat transmission and variable density to produce a refined product with the desired properties. Such factors are crucial, particularly in the metallurgical processes that include the purifying of molten metal from nonmetallic impurities and the cooling of continuous strips and filaments dragged through a quiescent fluid. There's no denying that the typical heat transfer fluids, such as water, mineral oils, and ethylene glycol, have low thermal conductivities. Therefore, a variety of approaches are used to increase the thermal conductivity of such fluids by suspending components in liquids that are micro sized. Developed by Maxwell for electromagnetism, magnetohydrodynamics is the dynamic study of electrically conducting fluid. A magnetic field has the capacity to induce currents in moving conducting fluid and some buoyancy forces to change the electromagnetic fields. This is the basic concept underlying an electrically conducting fluid.

Most of the research has been discovered with lower temperature difference and constant density between the ambient fluid and surface. But some problems are found with maximum temperature difference due to radiation. In this situation, the density is assumed as exponential function of temperature and fluid is assumed to be electromagnetic in the sense of ionized fluid due to the high operating temperature. Radiation effects on MHD nanofluid flow are very useful in the context of process involving high temperatures. In actuality, many processes in cutting edge engineering field takes place at high temperatures with the knowledge of radiation heat transfer for the design of the necessary machinery. The examples of such engineering field are nuclear power plants, gas turbines, and various propulsion systems for aircraft, missiles, satellites, and spacecraft. Due to the challenges involved to study these issues, relatively little is actually understood about how radiation affects the boundary layer flow of a nanofluid for radiating body. There are three significant challenges to the study of nanofluid radiation. First, it is highly challenging to estimate fluid absorption when radiating heat transfer occurs in a system. The radiation is absorbed and emitted not only at the system boundaries but also inside the system. Secondly, the wave length has a substantial influence on the absorption coefficients of the absorbing and emitting fluids in general. To calculate the radiating flux, a daunting amount of integration with respect to wavelength and other independent variables must be done. Third, adding the radiation factor to the energy equation creates a difficult to solve partial differential equation that is very nonlinear. In addition, important examples of fluid flows in the induced magnetic field include the flow of helium in pebble-bed nuclear reactors, underground disposal of nuclear or nonnuclear waste, food processing and storage, crude oil extraction, flow in the eyes of glaucoma patients, and flow through filtering media. Due to the difference in viscosity between a nanofluid and a magnetic field, the Lorentz force effects provide resistance to the nanofluid flow. Furthermore, the current issues have significant implications for the polymer industries, including paper production, glass-fiber production, liquid crystal solidification, petroleum production, production of unusual lubricants, suspension solutions, wire drawing, continuous cooling, fiber spinning, plastic film production, polymer sheet extraction, heat exchangers, petroleum resource recovery, fault zones, catalytic reactors, and the production of electronic devices.

The purpose of radiation effects in the thermal equation to enhance the temperature of the fluid flow domain in which heat transfer rate rises and the nanofluid serves the same purposes instead of using the transparent fluids like water simply. By the encountering the radiation, fluid becomes optically dense gray fluid. Here, the thermal radiation is used to enhance the surface temperature and nanofluid preserve the temperature of the fluid. So, the thermal radiation is just used as supporting agent due to exponentially temperature dependent density. Pourrajab and Noghrehabadi [1] illustrated bio convective mechanism of viscoelastic fluid across a stretching surface in a permeable material using kinetic temperature in the presence of microorganism. They found that the conductivity and Reynolds ratio increases the temperature profile with decreasing behavior. Sarkar and Endalew [2] elaborated the impacts of the crystallization on viscoelastic small fluid particles with MHD flow in a porous material. They observed that as the Nusselt number increases, the thickness of the temperature field decreases.

Kalavathamma and Lakshmi [3] studied the impact of various characteristics on mass and heat transfer of viscous fluid particles across a horizontal cylinder saturated in a permeable material. They found that the temperature profile distribution of the fluid decreases as the value of the Brownian motion parameter rises. Dero et al. [4] depicted the impacts of Darcy Forchheimer in a permeable material on the flow of radiation and magnetism over a decreasing hybrid shape. They deduced that the variable of copper volume concentration increases the thermal flow behavior. Srinivasacharya and Surender [5] analyzed the impacts of doubly stratification on free/forced convective boundary flow of viscous fluid particles across a vertical surface in a porous material. They obtained that the ratio of temperature and energy decreases significantly by increasing the Darcy number. Ayodeji et al. [6] developed flow separation impacts of mass particles of slip flow of fluid passing through a porous stretching material. They obtained that surface tension rises as the slip velocity increases as well as the mass slip falls. Khan and Pop [7] performed a tubular analysis on a laminar nanofluid problem form a stretching geometry. They observed that the Sherwood number is reduced by increasing the Pr.

Ghalambaz et al. [8] determined the physical flow of nanoparticle across a porous stretching surface. James et al. [9] developed a dynamic thickness of fluid particles through a conductive cylinder inserted in a porous material with heat energy. They observed that the thermal radiation parameter increases the Nusselt and Sherwood number across the stretching surface. The researcher [10] analyzed the effects of baffles on nanofluid-filled enclosures used in convective heat transfer. Entropy analysis on circular pseudo plastic flow with MHD by utilizing the Keller box approach is carried out numerically in [11]. The researcher [12] performed a numerical analysis of the effects of Reynolds on micropolar flow in a channel.

Rana and Bhargava [13] illustrated the mechanism of laminar fluid of nanoparticle across a quasi-stretched surface by using finite element method. Irfan et al. [14] constructed the MHD nanoliquid flow across a dynamic surface area by using numerical method having differ liquid properties. Ferdows et al. [15] studied free forced convective boundary flow of nanofluid particles across the porous material by using stretched shape. Mahabaleshwar et al. [18] presented an analytical approach on capturing the effect of incompressible, non-Newtonian, viscous, Casson nanofluid flow past a stretching/shrinking surface, under the influence of heat radiation and mass transfer parameter. Vishalakshi et al. [19] explained the 3-D MHD fluid flow under the impact of a magnetic field with an inclined angle. Maranna et al. [20] examined the impact of radiation and Marangoni convective boundary conditions on the flow of ternary hybrid nanofluid in a porous medium with mass transpiration effect. Again, Maranna et al. [21] investigated analytically a continuous stream of viscoelastic fluid and magnetohydrodynamic flow of second-grade fluids owing to protracted sheets in a permeable medium with the help of the Cattaneo–Christov pattern. Mahesh et al. [22] evaluated the single wall and multiwall carbon nanotube models to investigate the effect of suction and injection over a Marangoni boundary layer flow on magnetohydrodynamics (MHD) Casson fluid and thermal radiation on a permeable surface. Mahabaleshwar et al. [23] investigated the non-Newtonian MHD flow and heat transfer of copper-alumina/water hybrid nanofluid due to permeable stretching/shrinking surface with full slip model.

Singh et al. [24] discusses the laminar boundary layer flow of an electrically conducting Casson fluid due to a horizontal perforated sheet undergoing linear shrinking/stretching with mass transpiration. Dessie and Fissha [25] studied free forced convective flow of Maxwell nanofluid particles across a horizontal porous surface. Gireesha et al. [26] studied a numerical simulation for fluid particle suspension and MHD flow for heat transmission across a stretch sheet contained in a quasi permeable medium. They observed that the size of the atmospheric boundary layer is decreased by floating small dust particles in pure solution. Lakshmi et al. [27] investigated the solution of mass transfer of multiple particles produced by a continuously stretching surface by using RK-4 simulation. They concluded that the size of the energy, temperature, and chemical boundary regions reduces with higher nanoparticle concentration. In the numerical analysis with the effects of magnetohydrodynamics, reduce gravity, slip velocity and stratified medium on transient fluid over a non-conducting rotating geometry, the researchers [28–31] elaborated the fluctuations in the mass and heat characteristics.

Krishnaan and Chamkha [32] analyzed the impacts of Maxwell and ion drift on mixed convective mechanism of nanofluid flow particles across a stretched surface enclosed in a permeable medium. Prasannakumara et al. [33] investigated the Newtonian fluid solution with nanoparticle of MHD flow through a stretched surface placed in a permeable medium. Gireesha et al. [34] illustrated the viscoelastic fluid flow separation past a stretching surface filled with nanoparticles. They found that the temperature is enhanced with higher Prandtl number and the volumetric percentage of micro particles. The viscous dissipative, magnetohydrodynamics and radiations impacts on laminar fluid analysis along the stretching surface were examined by Maranna et al. [35]. For various engineering applications, Mabood et al. [36] carried out magnetohydrodynamics and entropy analysis for Jeffrey nanofluid phenomenon across the stretching surface. Rajesh et al. [37] analyzed the exact analytical solutions of hybrid nanofluid flow for heat transfer characteristics along the vertical infinite surface with ramped temperature. Liosis et al. [38] studied the combined form of shear and electromagnetic mixing to compute optimization mixing strategies under various initial conditions. The Carreau nanofluid phenomenon for concentration and heat characteristics with variable properties effects along stretchable surface has been considered in [39]. Ullah et al. [40] examined the heat rate analysis on electromagnetic vertical surface with MHD and thermal slip effects numerically. Jamshed et al. [41] investigated the transient magneto Williamson nanofluid flow along the plate with entropy generation effects numerically. Chamkha et al. [42–45] explored the solar radiation, heat generation/absorption, hydromagnetic, and thermophoresis effects on free convection along the vertical surface embedded in a porous medium numerically. The heat and mass transfer characteristics of natural convection boundary layer flow along the porous vertical and inclined surface under magnetic field has been evaluated in [46–49]. Damseh et al. [50] explored the study of combined heat and mass transfer by natural convection of a micropolar, viscous and heat generating or absorbing fluid flow near a continuously moving vertical permeable infinitely long surface in the presence of a first-order chemical reaction. Takhar et al. [51] studied the non-similar boundary layer flow of a viscous incompressible electrically conducting fluid over a moving surface in a rotating fluid, in the presence of a magnetic field, Hall currents and the free stream velocity. Wakif et al. [52] evaluated the electro-magneto-hydrodynamic convective flow features of a viscous electrically conducting fluid over a horizontal Riga plate by considering the wall suction and Joule heating effects. Maghari and Chamkha [53] investigated the problem for an infinite vertical plate numerically using the fourth-order Runge–Kutta method. By following these authors, many people believe that the nanotechnology is most important factor for the next large industrial revolution of this century. The nanofluid particles have great interest to manipulate the matter of molecular structure in order to innovate in almost every sector of the economy and in government projects, including national security, transportation, the environment, the medical and physical sciences as well as electronic cooling.

For the purpose of numerical analysis, the current mechanism on the rate of heat transfer and the rate of mass transfer along a stretching sheet with MHD, variable density and radiation effects is examined. The effects of variable density, MHD and radiation on heat and mass transfer of nanoparticle fraction phenomena of nanofluid across a stretching sheet with thermophoresis and Brownian motion have been investigated numerically by using the concept of previous research [7]. The non-similar expressions are numerically integrated with the Keller Box method. The numerical outcomes are deduced in graphs and tabular

form with the help of MATLAB program. The physical characteristics of emergent variables in the flow model, such as velocity graph, temperature field graph, and concentration graph, as well as their slopes, such as skin-friction rate, rate of heat transfer, and rate of mass transfer has been plotted. The novelty of the current work is to predict heat and mass transfer characteristics past a stretching sheet with MHD, thermal radiation and variable density effects for two phase fluid under thermophoresis and Brownian motion. Most of studies are found to deal with a small temperature difference between the surface and ambient fluid. However, the circumstances arise where this temperature difference is high due to radiation. In this situation, the density is assumed as exponential function of temperature and fluid is assumed to be electrically conducting in the sense of ionized fluid due to the high operating temperature. In the study of boundary layer theory several authors used finite difference scheme, implicit finite difference scheme. Sometimes differential equations are very difficult to solve analytically or models are needed for computer simulation. In these cases finite difference methods are used to solve these equations instead of analytical case. This is very accurate method and frequently used by researchers/scientists working in the field of boundary layer theory. So, finite difference method is very understandable and easiest when tackling the differential equations. Moreover, the performing of error analysis is very good through this method which is not trivially done via Taylor series expansions. The whole calculated mechanism is normal to the surface. The finite difference scheme is a valid, stable and frequently used technique to solve boundary value problems. By using Keller Box Scheme with standard Newton-Raphson technique, all appearance of powers of δ greater than the first power are neglected and difference equations are arranged in tri-diagonal matrix for algorithm. Here, we have taken $\eta_{max} = 10$ and $n = 401$ were taken for the convergence of numerical results rounded to 6 decimal places. The numerical and graphical results of $f'(\eta), \theta(\eta)$ and $\phi(\eta)$ as well as skin friction, heat transfer and mass transfer is accurate by satisfying the given boundary conditions. The findings of this research, to the best of our knowledge, are original and have never been published.

2. The flow geometry and mathematical formulation

The current mechanism is computed for numerical outcomes of the MHD, variable density and radiation impact on heat and mass transfer of nanoparticle fraction phenomena of nanofluid across a stretching sheet in a porous material with thermophoresis and Brownian motion effects. Using stream function forms, the extended issue will be reduced to a set of partial differential conditions, which will subsequently be converted into ordinary conditions. By incorporating the Keller Box approach with finite difference method (FDM), the molding issue will be solved. Graphical and tabular interpretations of the simulation solution for the material properties under analysis will be used.

By considering the incompressible, steady nanofluid in two dimensions in Fig. 1, u and v are the velocity fields in the x and y orders, respectively, where x and y are the axes parallel and perpendicular to the stretching porous sheet, temperature is denoted by T, free stream temperature T_∞, fluid thermal conductivity κ, and specific heat C_p respectively. The fluid density is represented with ρ, the density of particles is ρ_p, the kinematic fluid viscosity is $\nu = \mu/\rho$, the fluid density is the ρ_f, and the gravitational acceleration is the g. The mathematical equations for the current physical model by following [7,41] are given below;

$$\frac{\partial(\rho u)}{\partial x} + \frac{\partial(\rho v)}{\partial y} = 0 \tag{1}$$

$$\rho\left(u\frac{\partial u}{\partial x} + v\frac{\partial u}{\partial y}\right) = -\frac{\partial p}{\partial x} + \mu\left(\frac{\partial^2 u}{\partial x^2} + \frac{\partial^2 u}{\partial y^2}\right) + g(\rho_\infty - \rho) - \sigma^* {B_0}^2 u \tag{2}$$

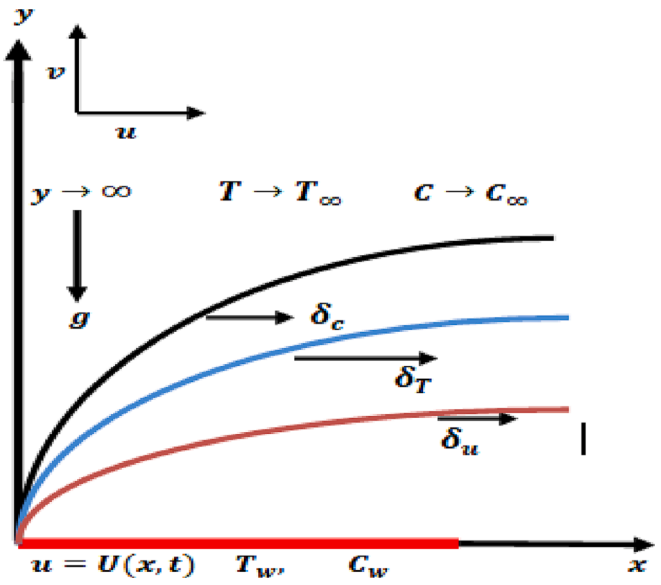

Fig. 1. Coordinate system and flow geometry.

$$\rho\left(u\frac{\partial v}{\partial x} + v\frac{\partial v}{\partial y}\right) = -\frac{\partial p}{\partial y} + \mu\left(\frac{\partial^2 v}{\partial x^2} + \frac{\partial^2 v}{\partial y^2}\right) + g(\rho_\infty - \rho) - \sigma^* {B_0}^2 v \tag{3}$$

$$(\rho c_p)_f\left(u\frac{\partial T}{\partial x} + v\frac{\partial T}{\partial y}\right) = \kappa\left(\frac{\partial^2 T}{\partial x^2} + \frac{\partial^2 T}{\partial y^2}\right) - \frac{\partial q_r}{\partial y} + (\rho c_p)_p\left\{D_B\left(\frac{\partial C}{\partial x}\frac{\partial T}{\partial x} + \frac{\partial C}{\partial y}\frac{\partial T}{\partial y}\right) + \left(\frac{D_T}{T_\infty}\right)\left[\left(\frac{\partial T}{\partial x}\right)^2 + \left(\frac{\partial T}{\partial y}\right)^2\right]\right\} \tag{4}$$

$$u\frac{\partial C}{\partial x} + v\frac{\partial C}{\partial y} = D_B\left(\frac{\partial^2 C}{\partial x^2} + \frac{\partial^2 T}{\partial y^2}\right) + \left(\frac{D_T}{T_\infty}\right)\left(\frac{\partial^2 T}{\partial x^2} + \frac{\partial^2 T}{\partial y^2}\right) \tag{5}$$

Boundary conditions of the present model by following [7,41] are,

$$v = 0, u = u_w(x) = ax, T = T_w, C = C_w \text{at} y = 0 \tag{6}$$

$u = v \to 0, T \to T_\infty, C \to C_\infty$ as $y \to \infty$.

The preceding description presents the appropriate boundary conditions for the temperature and velocity components. The P represents fluid pressure, ρ represents the density of the base fluid, α represents thermal diffusivity, ν represents kinematic viscosity,a represents a positive constant, D_B represents the Brownian diffusion coefficient, D_T represents the thermophoretic diffusion coefficient, and $\tau = (\rho c)p/(\rho c)f$ represents fluid heat capacity and nanoparticle materials heat capacity ratio, where ρ represents density, the $q_r = -16T^3{}_\infty \sigma \partial T/3\kappa^* \partial y$, σ being the Stephen Boltzmann constant, κ^* is absorption constant, and c represents the coefficient of volume expansion.

3. Stream functions and similarity variables

The appropriate unit less stream functions ψ and similarity variables to transform PDEs into ODEs by following [7] are given in Eqs. (7) and (8) with η and dimensionless temperature θ,

$$u = \frac{1}{\rho}\frac{\partial \psi}{\partial y}, v = -\frac{1}{\rho}\frac{\partial \psi}{\partial x}, \phi(\eta) = \frac{C - C_\infty}{C_w - C_\infty} p = p_o(constant) \tag{7}$$

$$\psi = (av)^{\frac{1}{2}} x f(\eta), \theta(\eta) = \frac{T - T_\infty}{T_w - T_\infty}, \eta = (a/v)^{1/2} y \tag{8}$$

The Eqs. (7) and (8) are used to turn the PDEs from Eqs. (1) to (6) into nonlinear ODEs;

$$\left(f^{'2}-ff''\right)=e^{-n\theta}(f'''-n\theta' f'')-\lambda\left(\frac{1-e^{n\theta}}{1-e^{-n}}\right)-e^{n\theta}\xi f' \tag{9}$$

$$\frac{e^{-n\theta}}{p_r}\left(\left(1+\frac{4}{3}R_d\right)\theta''-n\theta'^2\right)+f\theta'+\left(e^{-n\theta}\right)^2[N_B\phi'\theta'+N_T\theta'^2]=0 \tag{10}$$

$$\left(e^{-n\theta}\right)^2[(\phi''-n\phi'\theta')+\frac{N_T}{N_B}(\theta''-n\theta'^2)]+Lef\phi'=0 \tag{11}$$

where, $\Pr=\frac{\nu}{\alpha}$ is Prandtl parameter, $Le=\frac{\nu}{D_B}$ is Lewis parameter,$N_B=\frac{(\rho c)_p D_B(\phi_w-\phi_\infty)}{(\rho c)_f\nu}$ is a Brownian-motion number,$\xi=\frac{\sigma^* B_0{}^2 x}{\rho a}$ is the magnetic number,$n=\beta(T_w-T_\infty)$ is variable density number, $\lambda=Gr/Re^2$ is buoyancy number, dimensionless temperature is denoted by θ, kinematic viscosity is denoted by $\nu=\frac{\mu}{\rho}$, radiation is $R_d=\frac{4\sigma T^3_\infty}{\kappa\kappa^*}$ and $N_T=\frac{(\rho c)_p D_T(T_w-T_\infty)}{(\rho c)_f\nu T_\infty}$ is thermophoresis parameter. The boundary conditions in (6) then becomes,

$$f(\eta)=0,f'(\eta)=1,\theta(\eta)=1,\ \phi(\eta)=1\,\text{at}\,\eta=0 \tag{12}$$

$$f'(\infty)=0,\theta(\infty)=0,\phi(\infty)=0\ \text{at}\ \eta\to\infty.$$

4. Computational scheme and solution methodology

The connected mathematical nonlinear PDEs model is changed into similar ODEs model with similarity variables using an appropriate stream function formulation. In Eqs. (9) to (11), similar coupled ODEs model with given boundary conditions are solved using the iterative Keller Box approach (12). The additional independent quantities are introduced by $p(\eta);q(\eta),u(\eta),v(\eta),l(\eta)$ and $m(\eta)$ by using Eq. (13),

$$f'=p',f''=p'=\mathrm{q},f'''=q',\varphi'=u,\varphi''=u'=v,\varphi'''=v',\theta'=l,\theta''=l'=m \tag{13}$$

To overcome this issues, the Eqs. (9)–(12) becomes simple to solve with the straightforward forms,

$$f'=p\Rightarrow f'-p=0 \tag{14}$$

$$p'=q\Rightarrow p'-q=0 \tag{15}$$

$$\phi'=u\Rightarrow\phi'-u=0 \tag{16}$$

$$u'=v\Rightarrow u'-v=0 \tag{17}$$

$$\theta'=l\Rightarrow\theta'-l=0 \tag{18}$$

$$\left(p^2-\mathrm{fq}\right)=e^{-n\theta}(q'-nlq)-e^{-n\theta}\xi p-\lambda\left(\frac{1-e^{n\theta}}{1-e^{-n}}\right) \tag{19}$$

$$\frac{1}{p_r}((1+\frac{4}{3}R_d)m-nl^2)+fl+e^{-n\theta}[N_B ul+N_T l^2]=0 \tag{20}$$

$$\left(e^{-n\theta}\right)^2[(v-nlu)+\frac{N_T}{N_B}(m-nl^2)]+Lefu=0 \tag{21}$$

The reduced boundary conditions are,

$$f(0)=0,P(0)=1,\theta(0)=1,\varphi(0)=1,at\eta=0, \tag{22}$$

$$P(\infty)\to0,\theta(\infty)\to0,\varphi(\infty)\to0,as\eta\to\infty,$$

Now consider the midpoint values by following [40] with segment η_{n-1}, η_n with $\eta_{n-\frac{1}{2}}$ by using Eq. (23);

$$\eta_0=0,\eta_n=\eta_{n-1}+h_n,\eta_n=\eta_\infty \tag{23}$$

The above Eqs. (14) to (22) are transformed with average and central difference forms given in Eq. (24) by following [40],

$$f'=\frac{f_n-f_{n-1}}{h_n},f=\frac{f_n+f_{n-1}}{2}=f_{n-\frac{1}{2}} \tag{24}$$

and

$$f_n-f_{n-1}-\frac{1}{2}h_n\left(p_n+p_{n-1}\right)=0 \tag{25}$$

$$p_n-p_{n-1}-\frac{1}{2}h_n\left(q_n+q_{n-1}\right)=0 \tag{26}$$

$$\phi_n-\phi_{n-1}-\frac{1}{2}h_n(u_n+u_{n-1})=0 \tag{27}$$

$$u_n-u_{n-1}-\frac{1}{2}h_n(v_n+v_{n-1})=0 \tag{28}$$

$$\theta_n-\theta_{n-1}-\frac{1}{2}h_n(l_n+l_{n-1})=0 \tag{29}$$

$$\begin{aligned}\frac{1}{4}(p_n+p_{n-1})^2-\frac{1}{4}(f_n+f_{n-1})(q_n+q_{n-1})&=\frac{1}{2h_n}(2-n\theta_n+n\theta_{n-1})(q_n-q_{n-1})\\&-\frac{n}{8}(2-n\theta_n+n\theta_{n-1})(l_n+l_{n-1})(q_n+q_{n-1})\\&-\frac{\xi}{4}(2-n\theta_n+n\theta_{n-1})(p_n+p_{n-1})-\frac{\lambda}{2}(\theta_n+\theta_{n-1})\end{aligned} \tag{30}$$

$$\begin{aligned}\frac{1+\frac{4}{3}R_d}{2P_r}(m_n+m_{n-1})-\frac{n}{4P_r}(l_n+l_{n-1})^2+\frac{1}{4}(f_n+f_{n-1})(l_n+l_{n-1})\\+\frac{N_b}{8}(2-n\theta_n-n\theta_{n-1})(u_n+u_{n-1})(l_n+l_{n-1})\\+\frac{N_t}{8}(2-n\theta_n-n\theta_{n-1})(l_n+l_{n-1})^2=0\end{aligned} \tag{31}$$

$$\begin{aligned}1+\frac{n^2}{2}(\theta_n+\theta_{n-1})^2-n(\theta_n+\theta_{n-1})\left[\frac{1}{2}(v_n+v_{n-1})-\frac{n}{4}(l_n+l_{n-1})(u_n\right.\\\left.+u_{n-1})\right]\frac{N_T}{N_b}\left(\frac{1}{2}(m_n+m_{n-1})-\frac{n}{4}(l_n+l_{n-1})^2\right)+\frac{Lef}{2}(u_n+u_{n-1})\\=0\end{aligned} \tag{32}$$

along with boundary conditions

$$f_0=0,\ \phi_0=1,\ p_0=0,\ \theta_0=1,\ u=1,\ \text{at}\ \eta=0 \tag{33}$$

$$p_n\to0,\ \theta_n\to0,\ \phi_0\to0,\ as\eta\to\infty$$

Now by using the iterative Newton-Raphson method to convert the transformed ODEs for a smooth algorithm as described below in Eq. (34);

$$\begin{aligned}f_n^{k+1}=f_n^k+\delta f_n^k,p_n^{k+1}=p_n^k+\delta p_n^k,q_n^{k+1}=q_n^k+\delta q_n^k,\theta_n^{k+1}=\theta_n^k+\delta\theta_n^k,u_n^{k+1}\\=u_n^k+\delta u_n^k,\phi_n^{k+1}=\phi_n^k+\delta\phi_n^k,v_n^{k+1}=v_n^k+\delta v_n^k,l_n^{k+1}=l_n^k+\delta l_n^k\end{aligned} \tag{34}$$

Now by using the standard Newton-Raphson approach, the above converted equations are transformed into system of algebraic equations and then solved by generating the global matrix. The new transformed equations are,

$$\delta f_n-\delta f_{n-1}-\frac{1}{2}h_n(\delta p_n+\delta p_{n-1})=(r_1)_n \tag{35}$$

$$\delta p_n-\delta p_{n-1}-\frac{1}{2}h_n(\delta q_n+\delta q_{n-1})=(r_2)_n \tag{36}$$

$$\delta\phi_n-\delta\phi_{n-1}-\frac{1}{2}h_n(\delta v_n+\delta v_{n-1})=(r_3)_n \tag{37}$$

$$\delta u_n-\delta u_{n-1}-\frac{1}{2}h_n(\delta v_n+\delta v_{n-1})=(r_4)_n \tag{38}$$

$$\delta\theta_n - \delta\theta_{n-1} - \frac{1}{2}h_n(\delta l_n + \delta l_{n-1}) = (r_5)_n \tag{39}$$

The equations are given below in their condensed form, once more utilizing Eqs. (35) to (39) in Eqs. (30) to (33);

$$\begin{aligned}(a_1)_n\delta p_n + (a_2)_n\delta p_{n-1} + (a_3)_n\delta f_n + (a_4)_n\delta f_{n-1} + (a_5)_n\delta q_n + (a_6)_n\delta q_{n-1}\\ + (a_7)_n\delta\theta_n + (a_8)_n\delta\theta_{n-1} + (a_9)_n\delta l_n + (a_6)_n\delta l_{n-1} = (r_6)_n\end{aligned} \tag{40}$$

$$\begin{aligned}(b_1)_n\delta m_n + (b_2)_n\delta m_{n-1} + (b_3)_n\delta l_n + (b_4)_n\delta l_{n-1} + (b_5)_n\delta\theta_n + (b_6)_n\delta\theta_{n-1}\\ + (b_7)_n\delta u_n + (b_8)_n\delta g_{n-1} + (b_9)_n\delta f_n + (b_{10})_n\delta f_{n-1} = (r_7)_n\end{aligned} \tag{41}$$

$$\begin{aligned}(c_1)_n\delta\theta_n + (c_2)_n\delta\theta_{n-1} + (c_3)_n\delta v_n + (c_4)_n\delta v_{n-1}(c_5)_n\delta l_n + (c_6)_n\delta l_{n-1}\\ + (c_7)_n\delta f_n + (c_8)_n\delta f_{n-1} + (c_9)_n\delta u_n + (c_{10})_n\delta u_{n-1} = (r_8)_n\end{aligned} \tag{42}$$

Recalling the precise boundary conditions without iteration, we take steps to make sure that these correct values are preserved across all iterations.

$$\delta f_0 = 0, \delta\phi_0 = 1, \delta p_0 = 1, \delta\theta_0 = 1 \tag{43}$$

$$\delta p_n = 0, \delta\theta_n = 0, \delta\phi_n = 0$$

5. Matrix form of vector equations

The matrix based structure of the aforementioned difference equations is a crucial next step. If it's done incorrectly, the strategy either becomes incredibly ineffective since the matrix has no visible structure or zero solutions due to a solitary matrix with zero determinant or submatrix. The matrix form of vector equations is given as;

$$A\delta = r \tag{44}$$

$$[A] = \begin{bmatrix} \frac{[A_1][C_1]}{[B_2][A_2][C_2]} & \cdots & \cdots \\ \vdots & \ddots & \vdots \\ \vdots & \cdots & \frac{[B_{n-1}][A_{n-1}][C_{n-1}]}{[B_n][A_n]} \end{bmatrix}, [\delta] = \begin{bmatrix} [\delta_1] \\ [\delta_2] \\ \vdots \\ [\delta_{n-1}] \\ [\delta_n] \end{bmatrix}, [r]$$

$$= \begin{bmatrix} [r_1] \\ [r_2] \\ \vdots \\ [r_{n-1}] \\ [r_n] \end{bmatrix} \tag{45}$$

6. Quantitative and physical reasoning

Due to excessive heating, various physical problems are less interested in modern technologies and industries. The current physical phenomena addressed the variable density, MHD and radiation impact on heat and mass transfer of nanoparticle fraction phenomena of nanofluid across a stretching sheet with thermophoresis and Brownian motion effects has been explored numerically. The coupled partial differential equations of the present nanofluid mechanism are changed in nonlinear coupled ordinary differential equations with defined stream functions and similarity variables for smooth algorithm and integration. The changed ODEs are again converted in similar form for numerical outcomes by applying Keller Box approach. The numerical outcomes are deduced in graphs and tabular form with the help of MATLAB program. It is examined how physical quantities like as velocity graphs, temperature graphs, and concentration graphs behave together with their slopes, which represent the rates of mass transfer, heat transfer, and skin friction under the influence of various flow model parameters. The impact of physical parameters such as Prandtl parameter Pr, temperature density number n, Lewis parameter L_e, thermophoresis parameter Nt, buoyancy number λ, Brownian-motion number Nb, radiation number R_d and magnetic number ξ are drafted in numerical and physical form.

The Fig. 2a – c shows the impact of radiation number on the velocity graph, temperature graph and concentration graph respectively. The Fig. 2(a) shows the physical quantity of velocity graph for various values of $R_d = 1.0, 3.0, 5.0, 7.0, 9.0$. It is deduced that velocity graph is declined for minimum value of $R_d = 1.0$ and enhanced for higher value of $R_d = 9.0$ with $\lambda = 6.1$. This occurs because a rising buoyancy parameter value tends to increase temperature-dependent density variation and buoyancy force. It is noted that temperature θ plot is increased for higher value of $R_d = 9.0$ and reduced for lowest value of $R_d = 1.0$ in Fig. 2b. The presence of radiation in the layer has a tendency to reduce the enthalpies, their slopes, and increase the thickness of the thermal boundary layer as compared to the non-radiating case. This is because the radiation parameter's bigger value which is correlated with boundary layer thickness provided more heat to the working fluid within the boundary layer region. The prominent variation is noted in temperature plot against R_d. In Fig. 2c, the fluid concentration profile is enhanced for minimum $R_d = 1.0$ and reduced for higher $R_d = 9.0$ for Pr = 7.0. Physically, this is feasible since a rise in Pr reduces the thermal conductivity of nanofluid, which therefore reduces the amount of the shear stresses between the elastic regions. Fig. 3a – c illustrate the effect of different values of $\xi = 2.0, 5.0, 7.0, 9.0, 12.0$ on velocity U, temperature θ and concentration ϕ profile. In Fig. 3a it is seen that velocity U profile is increased at minimum of $\xi = 2.0$ and reduced for highest $\xi = 12.0$ with good response. The nanofluid flow is accelerated by an increasing value of the buoyancy parameter, acting as a supportive driving force that also greatly increases the movement within the flow separation. The Fig. 3b represents the effect of ξ on the $\theta(\eta)$ graph. It can be seen that temperature profile is reduced for lower $\xi = 2.0$ but increased by increasing $\xi = 12.0$. This outcome was anticipated since a rise in the magnetic force parameter corresponds to a rise in the Friction force, which resists the flow and thus causes a fall in the nanofluid velocity. On the other hand, the nanofluid demonstrates resistance to the Lorentz force as the force grows by increasing resistance between its layers. Fig. 3c indicates the effect of ξ on various value of $\phi(\eta)$ plot. It is examined that the concentration profile increased by increasing$\xi = 12.0$ but decreased by decreasing $\xi = 1.0$ in Fig. 3c. The prominent variation in every plot is noted for various choice of magnetic force number ξ. The Fig. 4a – c demonstrated the physical plots of velocity U, temperature θ and concentration ϕ plots for diverse $n = 0.0, 0.1, 0.3, 0.5, 0.7$. In Fig. 4(a), it is noted that velocity U plot is enhanced for minimum $n = 0.0$ and reduced for maximum $n = 0.7$. Fig. 4b illustrated the temperature profile along η. It should be observed that the density variation is insignificant as n approaches 0 except in the buoyant term, and it increases greatly as n takes values far higher than 0. It is deduced that $\theta(\eta)$ of fluid is decreased with the enhancement of n. Because of increased buoyancy forces, an increase in the density/temperature parameter n leads to a greater in the velocity of the nanofluid particles (the density variation with temperature increases). Fig. 4c displays the impact of density n on concentration graph which is decreased by increasing $n = 0.7$ but increased by decreasing $n = 0.0$. The prominent variation in every graph is noted for various choices of density n. Therefore, when n grows, two forces will be acting on the nanofluid velocity: the first force, caused by an increase in buoyancy forces, will cause the nanofluid velocity to increase, while the second force, caused by a reduction in temperature, will cause the nanofluid velocity to reduction. Fig. 5a and b presented the physical outcomes of heat transfer $\theta'(0)$ and mass transfer $\phi'(0)$ plots for $N_b = 0.1, 0.3, 0.5, 0.7$. It is noted the heat transfer $\theta'(0)$ is enhanced for minimum $N_b = 0.1$ and reduced for higher $N_b = 0.7$ by keeping fixed other parameters in Fig. 5b. It is found that a decrease in the concentration of nanoparticle is caused by larger values of Lewis number Le. The heat transfer $\theta'(0)$ graph is enhanced for maximum $N_b = 0.7$ and other value of N_b the heat transfer $\theta'(0)$ plot is similar in Fig. 5a. The prominent

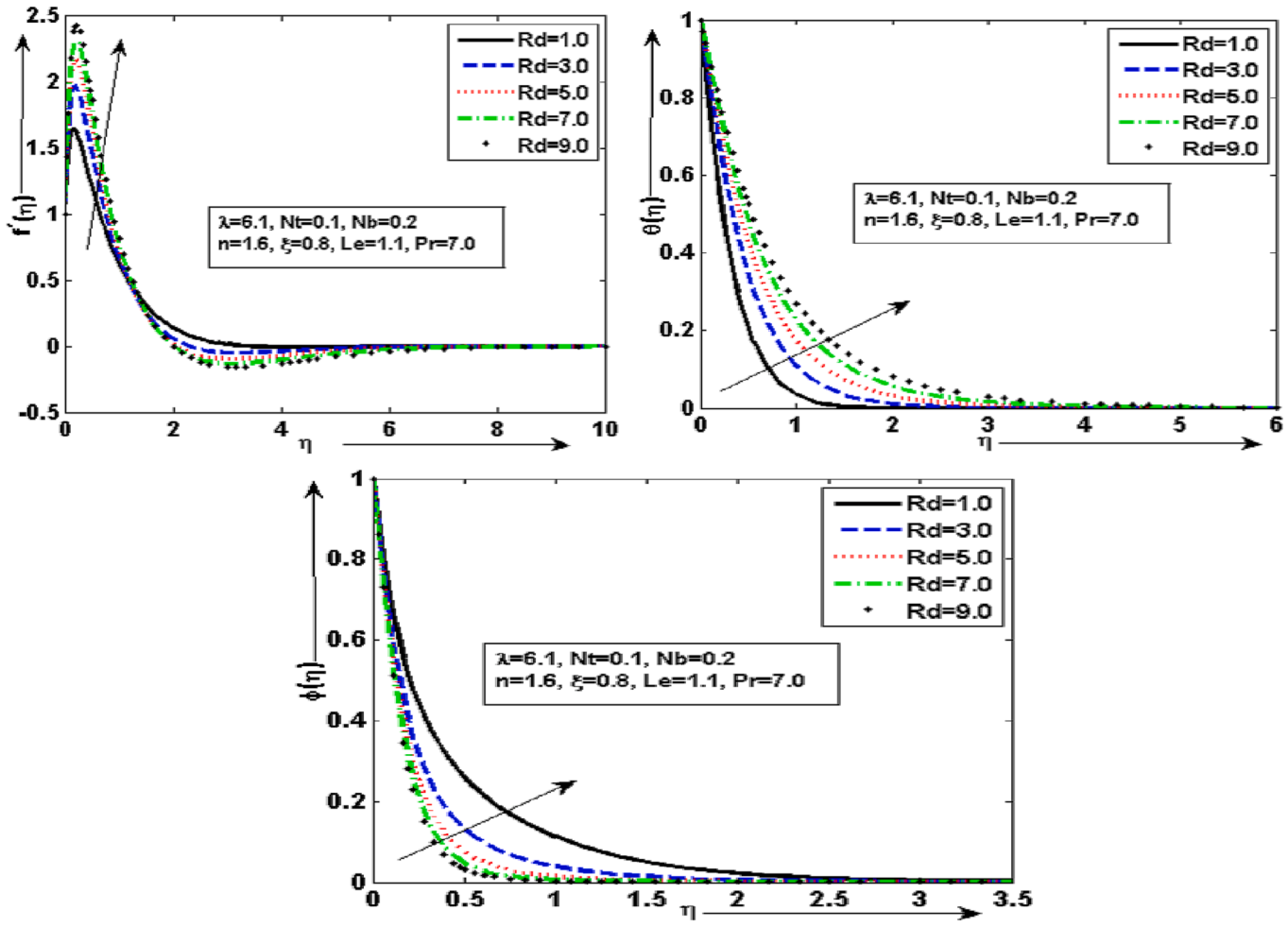

Fig. 2. (a)-2(c). Graphical plots of velocity $f'(\eta)$, temperature θ and concentration ϕ for some choices of $R_d = 1.0, 3.0, 5.0, 7.0, 9.0$ with some fixed parameters $\lambda = 6.1$, $Nt = 0.1$, $Nb = 0.2$, $n = 1.6$, $Le = 1.1$ and Pr = 7.0.

variation in every plot is noted for various porous number N_b. The heat rate is enhanced for maximum $N_t = 1.0$ with prominent variations and the lower heat rate is deduced for minimum $N_t = 0.1$. The temperature gradient in the inner region of thick boundary layer cannot be predicted correctly by the use of thick approximation alone except for thermal radiation parameter $Rd \gg 1$. It was expected because a bigger value of N_t causes a stronger thermophoresis force in the near-wall region, which raises the concentration of nanoparticle. It can be seen that the concentration rate is raised for higher $N_t = 1.0$ and the lower concentration rate is noticed for lower $N_t = 0.1$ with prominent variations. Fig. 6.

From the Table.1, it can be seen that skin-friction $f''(0)$ is enhanced for large $n = 1.0$ and the minimum skin-friction $f''(0)$ is deduced for small $n = 0.0$ under the influence of buoyancy parameter$\lambda = 1.5$. The heat rate $-\theta'(0)$ is enhanced for larger $n = 1.0$ and the minimum heat transfer is computed for smaller $n = 0.0$ with buoyancy parameter $\lambda = 1.5$. The mass transfer is maximum for larger $n = 1.0$ and the minimum mass transfer is noticed for smaller $n = 0.0$ with buoyancy parameter$\lambda = 1.5$. The Table 2 is indicated for the impact of ξ parameter for some choices $\xi = 0.5, 1.5, 2.0$ and 3.5 past a stretching sheet for physical characteristics of $f''(0), -\phi'(0)$ and $-\theta'(0)$ past the stretching surface with some constant $\lambda = 1.7$, $\xi = 3.5$ and $Pr = 7.0$. The skin friction $f''(0)$ is enhanced for lower $\xi = 0.5$ while the minimum value of skin-friction is examined for maximum $\xi = 2.5$. It is mentioned that heat rate is increased by decreasing $\xi = 0.5$ and reduced by increasing $\xi = 2.5$. The mass rate transfer is raised for lower choice of $\xi = 0.5$ while the lowest value of mass transfer is examined for larger value of $\xi = 2.5$. The Table 3 is presenting the comparison of heat transfer $-\theta'(0)$ with Wang [16], and Gorla and Sidawi [17] by reducing *Nt* and *Nb* effects for seven values of Prandtl number $\mathrm{Pr} = 0.07, 0.20, 0.70, 2.0, 7.0, 20.0, 70.0$in the presence of temperature density impact past the stretchy heated sheet. It is deduced that the prominent heat transfer is obtained with temperature dependent density effects for each Pr. Therefore, the current heat transfer results are accurate with the previous results.

7. Conclusion

In the present mechanism, the MHD, variable density and radiation impact on heat-mass transfer and nanoparticle fraction phenomena of nanofluid across stretching sheet with thermophoresis and Brownian motion effects has been explored numerically. The coupled partial differential equations of the present nanofluid mechanism are changed in nonlinear coupled ordinary differential equations with defined stream functions and similarity variables for smooth algorithm and integration. The changed ODEs are again converted in similar form for numerical outcomes by applying Keller Box approach. The numerical outcomes are deduced in graphs and tabular form with the help of MATLAB program. It is examined how physical quantities like as velocity graphs, temperature graphs, and concentration graphs behave together with their slopes, which represent the rates of mass transfer, heat transfer, and skin friction under the influence of various flow model parameters. The range of parameters has selected according as Prandtl number $0.07 \leq Pr \leq 70.0$, buoyancy parameter $0 < \xi < \infty$ and the choice of magnetic force parameter set the effects of magnetic diffusion and

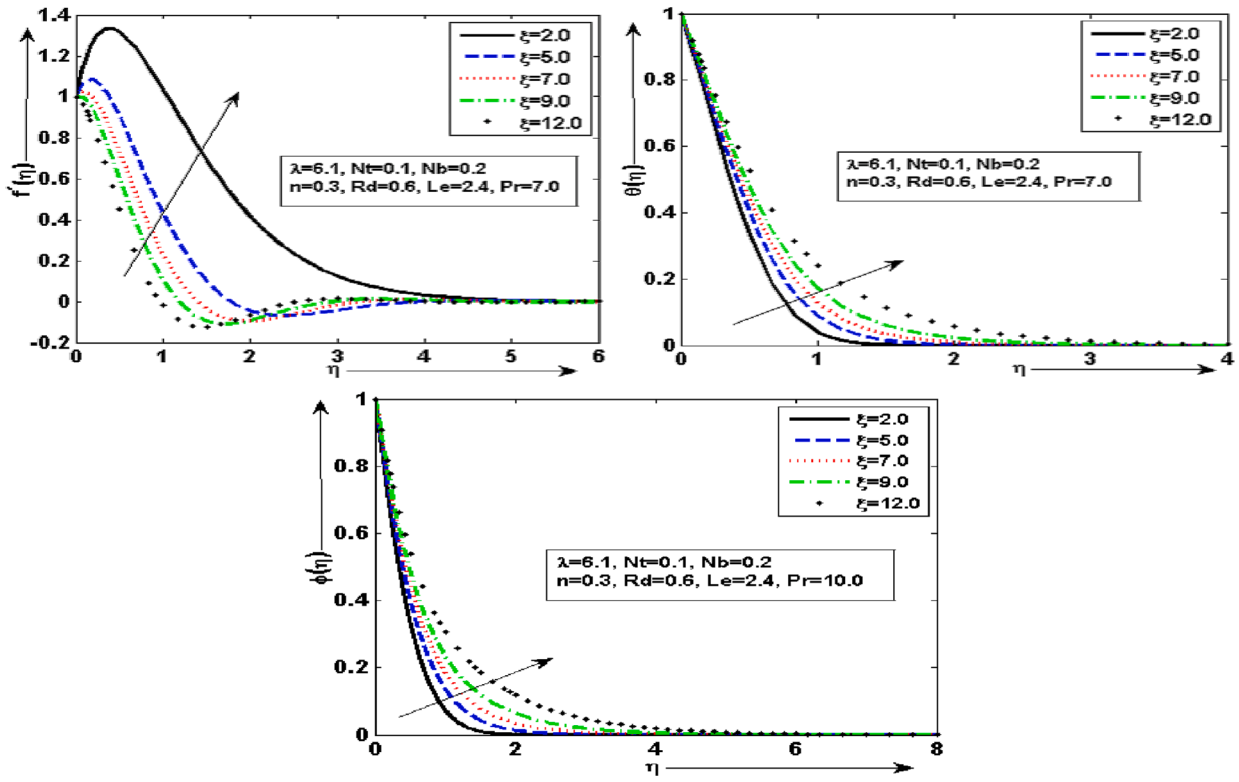

Fig. 3. (a)-3(c). Graphical plots of velocity $f'(\eta)$, temperature θ and concentration ϕ for some choices of $\xi = 2.0, 5.0, 7.0, 9.0, 12.0$ with some fixed parameters $\lambda = 6.1$, $Nt = 0.1$, $Nb = 0.2$, $n = 0.3$, $Le = 2.4$ and $\Pr = 7.0$.

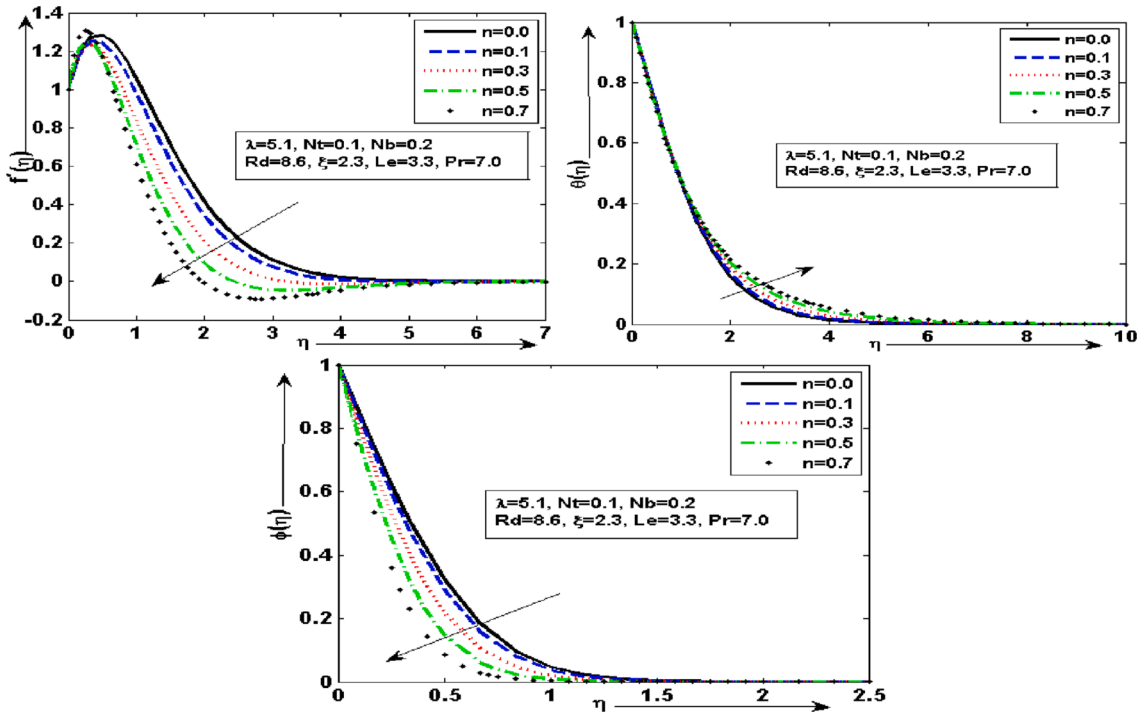

Fig. 4. (a)-4(c). Graphical plots of velocity $f'(\eta)$, temperature θ and concentration ϕ for some choices of $n = 0.0, 0.1, 0.3, 0.5, 0.7$ with some fixed parameters $\lambda = 5.1$, $Nt = 0.1$, $Nb = 0.2$, $Rd = 8.6$, $Le = 3.3$ and $\Pr = 7.0$.

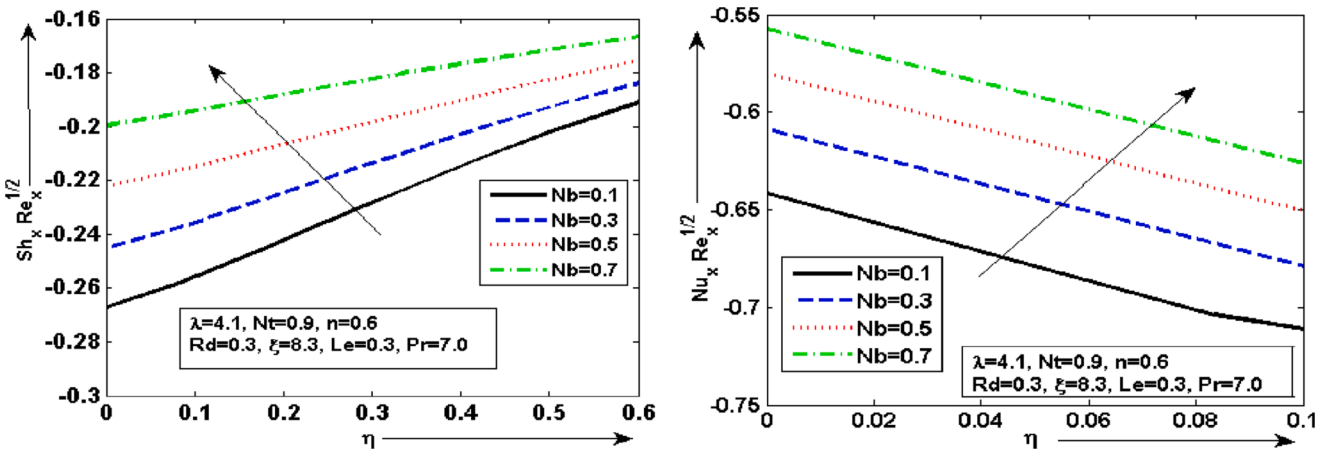

Fig. 5. (a)-5(c). Graphical plots of heat transfer $\theta'(0)$ and mass transfer $\phi'(0)$ for some choices of $Nb = 0.1, 0.3, 0.5, 0.7$ with some fixed parameters $\lambda = 4.1$, $Nt = 0.9$, $Rd = 0.3$, $n = 0.6$, $Le = 0.3$ and $\mathrm{Pr} = 7.0$.

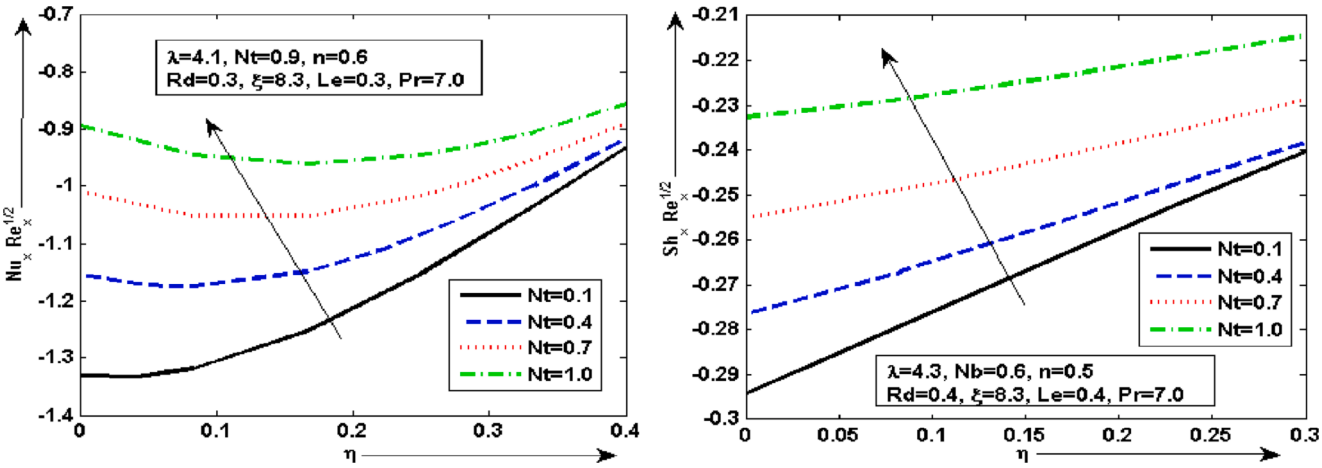

Fig. 6. (a)-6(c). Graphical plots of heat transfer $\theta'(0)$ and mass transfer $\phi'(0)$ for some choices of $Nt = 0.1, 0.4, 0.7, 1.0$ with some fixed parameters $\lambda = 4.3$, $Nb = 0.6$, $Rd = 0.4$, $n = 0.5$, $Le = 0.4$ and $\mathrm{Pr} = 7.0$.

Table 1
Numerical results for $f''(0), -\theta'(0)$ and for $-\phi'(0)$ for various values of $n = 0.0, 0.3, 0.6, 1.0$, while other parameters are fixed.

$n =$	$f''(0)$	$-\theta'(0)$	$-\phi'(0)$
0.0	4.879240614576633	0.174622809744148	1.514028648228383
0.3	5.553517239574258	0.282093810281554	1.929879513656921
0.6	7.128708418082393	0.451526060701176	2.503545641529655
1.0	11.14056359516007	0.828854931906472	3.609754807395438

Table 2
The numerical outcomes of $f''(0), -\theta'(0)$ and $-\phi'(0)$ with some choicΞes of $\xi. = 0.5, 1.5, 2.0, 3.5$.

	$f''(0)$	$-\theta'(0)$	$-\phi'(0)$
0.5	9.540455671088386	3.024123755289357	2.291019891109566
1.5	8.487572033095056	2.944285424442383	2.085276681324071
2.0	8.086105381985982	2.913421437893619	1.987179978853624
3.5	7.737145446285837	2.886620197701986	1.890161615731341

magnetic energy respectively. It is deduced that velocity graph is declined for minimum $R_d = 1.0$ and enhanced for higher $R_d = 9.0$. It is noted that temperature θ plot is increased for highest $R_d = 9.0$ and reduced for lowest $R_d = 1.0$. The velocity within the flow separation dramatically increases as the buoyancy parameter's value rises, acting as a supporting driving force to accelerate the nanofluid flow. Therefore,

Table 3
Comparison of numerical results for $-\theta'(0)$ heat transfer for various values of $Pr = 0.07, 0.20, 0.70, 2.0, 7.0, 20.0, 70.0$ with temperature density effects past the stretching porous sheet.

Pr	Gorla and Sidawi [16]	Wang [17]	Present Analysis
0.07	0.0656	0.0656	0.0868
0.20	0.1691	0.1691	0.1835
0.70	0.5349	0.4539	0.5196
2.0	0.9114	0.9114	0.9632
7.0	1.8905	1.8954	1.9364
20.0	3.3539	3.3539	3.3905
70.0	6.4622	6.4622	6.4962

when n grows, two forces will be acting on the nanofluid velocity: the first force, caused by an increase in buoyancy forces, will cause the nanofluid velocity to increase, while the second force, caused by a reduction in temperature, will cause the nanofluid velocity to reduction. It is concluded that the maximum choice of Lewis parameter Le causes a reduction in the nanoparticle concentration.

Declaration of Competing Interest

The authors declare that they have no known competing financial interests or personal relationships that could have appeared to influence the work reported in this paper.

Data availability

The data that has been used is confidential.

Acknowledgements

The author would like to extend his appreciation to the Deanship of Scientific Research at King Khalid University, Saudi Arabia for the funding this work through the Research Group Program under grant no. RGP.2/78/44.

References

[1] R. Pourrajab, A. Noghrehabadi, V.V. Koryanov, M. Polyakova, H. Yuan, Bioconvection of nanofluid past stretching sheet in a porous medium in presence of gyrotactic microorganisms with newtonian heating, MATEC Web Conf. 220 (2018) 01004.
[2] S. Sarkar, M.F. Endalew, Effects of melting process on the hydromagnetic wedge flow of a Casson nanofluid in a porous medium, Boundary Value Problems 2019 (1) (2019) 1–14.
[3] B. Kalavathamma, C. Lakshmi, Effect of variable properties on heat and mass transfer flow of nanofluid over a vertical cone saturated by porous medium under enhanced boundary conditions, Int. J. Appl. Eng. Res 13 (2018).
[4] S. Dero, H. Shaikh, G.H. Talpur, I. Khan, S.O. Alharbim, M. Andualem, Influence of a Darcy-Forchheimer porous medium on the flow of a radiative magnetized rotating hybrid nanofluid over a shrinking surface, Scientific Reports 11 (1) (2021) 1–16.
[5] D. Srinivasacharya, O. Surender, Effect of double stratification on mixed convection boundary layer flow of a nanofluid past a vertical plate in a porous medium, Applied Nanoscience 5 (1) (2015) 29–38.
[6] Ayodeji, F., Abubakar, A. A., & Joy-Felicia, O. O. Effect of Mass and Partial Slip on Boundary Layer Flow of a Nanofluid over a Porous Plate Embedded In a Porous Medium.
[7] W.A. Khan, I. Pop, Boundary-layer flow of a nanofluid past a stretching sheet, International journal of heat and mass transfer 53 (11–12) (2010) 2477–2483.
[8] M. Ghalambaz, A. Noghrehabadi, A. Ghanbarzadeh, Natural convection of nanofluids over a convectively heated vertical plate embedded in a porous medium, Brazilian Journal of Chemical Engineering 31 (2) (2014) 413–427.
[9] M. James, E.W. Mureithi, D. Kuznetsov, Effects of variable viscosity of nanofluid flow over a permeable wedge embedded in saturated porous medium with chemical reaction and thermal radiation, International Journal of Advances in Applied Mathematics and Mechanics 2 (3) (2015) 101–118.
[10] K. Al-Farhany, B. Al-Muhja, K. Loganathan, U. Periyasamy, F. Ali, I.E. Sarris, Analysis of Convection Phenomenon in Enclosure Utilizing Nanofluids with Baffle Effects, Energies 15 (18) (2022) 6615.
[11] Q. Al-Mdallal, V.R. Prasad, H.T. Basha, I. Sarris, N. Akkurt, Keller box simulation of magnetic pseudoplastic nano-polymer coating flow over a circular cylinder with entropy optimisation, Computers & Mathematics with Applications 118 (2022) 132–158.
[12] G. Sofiadis, I. Sarris, Reynolds number effect of the turbulent micropolar channel flow, Physics of Fluids 34 (7) (2022) 075126.
[13] P. Rana, R. Bhargava, Flow and heat transfer of a nanofluid over a nonlinearly stretching sheet: a numerical study, Communications in Nonlinear Science and Numerical Simulation 17 (1) (2012) 212–226.
[14] M. Irfan, M.A. Farooq, T. Iqra, A new computational technique design for EMHD nanofluid flow over a variable thickness surface with variable liquid characteristics, Frontiers in Physics 8 (2020) 66.
[15] M. Ferdows, M.S. Khan, M.M. Alam, S. Sun, MHD Mixed Convective Boundary Layer Flow of a Nanofluid through a Porous Medium due to an Exponentially Stretching Sheet, Mathematical Problems in Engineering 2012 (2012) 1–21.
[16] C.Y. Wang, Free convection on a vertical stretching surface, J. Appl. Math. Mech. (ZAMM) 69 (11) (1989) 418–420.
[17] R.S. Reddy Gorla, I. Sidawi, Free convection on a vertical stretching surface with suction and blowing, Appl. Sci. Res. 52 (3) (1994) 247–257.
[18] U.S. Mahabaleshwar, T. Maranna, F. Sofos, Analytical investigation of an incompressible viscous laminar Casson fluid flow past a stretching/shrinking sheet, Scientific Reports 12 (1) (2022) 18404.
[19] A.B. Vishalakshi, T. Maranna, U.S. Mahabaleshwar, D. Laroze, An effect of MHD on non-Newtonian fluid flow over a porous stretching/shrinking sheet with heat transfer, Applied Sciences 12 (10) (2022) 4937.
[20] T. Maranna, U.S. Mahabaleshwar, M.I. Kopp, The Impact of Marangoni Convection and Radiation on Flow of Ternary Nanofluid in a Porous Medium with Mass Transpiration, Journal of Applied and Computational Mechanics 9 (2) (2023) 487–497.
[21] Maranna, T., Sneha, K. N., Mahabaleshwar, U. S., & Souayeh, B. An impact of heat and mass transpiration on magnetohydrodynamic viscoelastic fluid past a permeable stretching/shrinking sheet. *Heat Transfer*.
[22] R. Mahesh, U.S. Mahabaleshwar, E.H. Aly, O. Manca, An impact of CNTs on an MHD Casson Marangoni boundary layer flow over a porous medium with suction/injection and thermal radiation, International Communications in Heat and Mass Transfer 141 (2023) 106561.
[23] U.S. Mahabaleshwar, E.H. Aly, T. Anusha, MHD slip flow of a Casson hybrid nanofluid over a stretching/shrinking sheet with thermal radiation, Chinese Journal of Physics 80 (2022) 74–106.
[24] J. Singh, A.B. Vishalakshi, U.S. Mahabaleshwar, G. Bognar, N.B. Khan, MHD Casson fluid flow with Navier's and second order slip due to a perforated stretching or shrinking sheet, Plos one 17 (11) (2022) e0276870.
[25] H. Dessie, D. Fissha, MHD Mixed Convective Flow of Maxwell Nanofluid Past a Porous Vertical Stretching Sheet in Presence of Chemical Reaction, Applications and Applied Mathematics: An International Journal (AAM) 15 (1) (2020) 31.
[26] B.J. Gireesha, B. Mahanthesh, P.T. Manjunatha, R.S.R. Gorla, Numerical solution for hydromagnetic boundary layer flow and heat transfer past a stretching surface embedded in non-Darcy porous medium with fluid-particle suspension, Journal of the Nigerian Mathematical Society 34 (3) (2015) 267–285.
[27] K.K. Lakshmi, B.J. Gireesha, R.S. Gorla, B. Mahanthesh, Effects of diffusion-thermo and thermo-diffusion on two-phase boundary layer flow past a stretching sheet with fluid-particle suspension and chemical reaction: A numerical study, Journal of the Nigerian Mathematical Society 35 (1) (2016) 66–81.
[28] Z. Ullah, M. Ashraf, A. Rashad, Magneto-thermo analysis of oscillatoryflow around a non-conducting horizontal circular cylinder, Journal of ThermalAnalysis & Calorimetry 142 (4) (2020).
[29] H. Waqas, M. Oreijah, K. Guedri, S.U. Khan, S. Yang, S. Yasmin, M.I. Khan, O. T. Bafakeeh, E.S.M. Tag-ElDin, A.M. Galal, Gyrotactic Motile Microorganisms Impact on Pseudoplastic Nanofluid Flow over a Moving Riga Surface with Exponential Heat Flux, Crystals 12 (2022) 1308.
[30] Z. Ullah, M. Ashraf, S. Zia, Y. Chu, I. Khan, K.S. Nisar, Computational analysis of the oscillatory mixed convection flow along a horizontalcircular cylinder in thermally stratified medium. *CMC*, Comput. Mater. Continua 65 (1) (2020) 109 {123.
[31] Z. Ullah, M. Ashraf, I.E. Sarris, T.E. Karakasidis, The Impact of Reduced Gravity on Oscillatory Mixed Convective Heat Transfer around a Non-Conducting Heated Circular Cylinder, Applied Sciences 12 (10) (2022) 5081.
[32] M. Veera Krishna, A.J. Chamkha, Hall and ion slip effects on MHD rotating boundary layer flow of nanofluid past an infinite vertical plate embedded in a porous medium, Results in Physics 15 (2019) 102652.
[33] B.C. Prasannakumara, N.S. Shashikumar, P. Venkatesh, Boundary layer flow and heat transfer of fluid particle suspension with nanoparticles over a nonlinear stretching sheet embedded in a porous medium, Nonlinear Engineering 6 (3) (2017) 179–190.
[34] B.J. Gireesha, B. Mahanthesh, R.S.R. Gorla, Suspended particle effect on nanofluid boundary layer flow past a stretching surface, Journal of nanofluids 3 (3) (2014) 267–277.
[35] T. Maranna, K.N. Sneha, U.S. Mahabaleshwar, I.E. Sarris, T.E. Karakasidis, An Effect of Radiation and MHD Newtonian Fluid over a Stretching/Shrinking Sheet with CNTs and Mass Transpiration, Applied Sciences 12 (11) (2022) 5466.
[36] F. Mabood, E.O. Fatunmbi, L. Benos, I.E. Sarris, Entropy Generation in the Magnetohydrodynamic Jeffrey Nanofluid Flow Over a Stretching Sheet with Wide Range of Engineering Application Parameters, International Journal of Applied and Computational Mathematics 8 (3) (2022) 1–18.
[37] V. Rajesh, M.A. Sheremet, H.F. Öztop, Impact of hybrid nanofluids on MHD flow and heat transfer near a vertical plate with ramped wall temperature, Case Studies in Thermal Engineering 28 (2021) 101557.
[38] Liosis, C., Karvelas, E., Karakasidis, T., & Sarris, I. (2022). Mixing of Fe3O4 nanoparticles under electromagnetic and shear conditions for wastewater treatment applications. *Journal of Water Supply: Research and Technology-Aqua*.
[39] N.Z. Basha, K. Vajravelu, F. Mebarek-Oudina, I. Sarris, K. Vaidya, K.V. Prasad, C. Rajashekhar, MHD Carreau nanoliquid flow over a nonlinear stretching surface, Heat Transfer 51 (6) (2022) 5262–5287.
[40] Z. Ullah, M. Bilal, I.E. Sarris, A. Hussanan, MHD and Thermal Slip Effects on Viscous Fluid over Symmetrically Vertical Heated Plate in Porous Medium: Keller Box Analysis, Symmetry 2022 (14) (2022) 2421.
[41] W. Jamshed, M.R. Eid, F. Shahzad, R. Safdar, M.D. Shamshuddin, Keller box analysis for thermal efficiency of magneto time-dependent nanofluid flowing in solar-powered tractor application applying nano-metal shaped factor, Waves in Random and Complex Media (2022) 1–36.
[42] A.J. Chamkha, C. Issa, K. Khanafer, Natural convection from an inclined plate embedded in a variable porosity porous medium due to solar radiation, International Journal of Thermal Sciences 41 (1) (2002) 73–81.
[43] A.J. Chamkha, A.R.A. Khaled, Similarity solutions for hydromagnetic simultaneous heat and mass transfer by natural convection from an inclined plate with internal heat generation or absorption, Heat and Mass Transfer 37 (2–3) (2001) 117–123.
[44] A.J. Chamkha, I. Pop, Effect of thermophoresis particle deposition in free convection boundary layer from a vertical flat plate embedded in a porous medium, International communications in heat and mass transfer 31 (3) (2004) 421–430.
[45] A.J. Chamkha, A.F. Al-Mudhaf, I. Pop, Effect of heat generation or absorption on thermophoretic free convection boundary layer from a vertical flat plate embedded in a porous medium, International Communications in Heat and Mass Transfer 33 (9) (2006) 1096–1102.
[46] A.J. Chamkha, A.R.A. Khaled, Hydromagnetic combined heat and mass transfer by natural convection from a permeable surface embedded in a fluid-saturated porous medium, International Journal of Numerical Methods for Heat & Fluid Flow 10 (5) (2000) 455–477.
[47] A. Chamkha, R.S.R. Gorla, K. Ghodeswar, Non-similar solution for natural convective boundary layer flow over a sphere embedded in a porous medium saturated with a nanofluid, Transport in porous media 86 (1) (2011) 13–22.

[48] A.J. Chamkha, Hydromagnetic natural convection from an isothermal inclined surface adjacent to a thermally stratified porous medium, International Journal of Engineering Science 35 (10–11) (1997) 975–986.
[49] Chamkha, A. J. (1997). Solar radiation assisted natural convection in uniform porous medium supported by a vertical flat plate.
[50] R.A. Damseh, M.Q. Al-Odat, A.J. Chamkha, B.A. Shannak, Combined effect of heat generation or absorption and first-order chemical reaction on micropolar fluid flows over a uniformly stretched permeable surface, International Journal of Thermal Sciences 48 (8) (2009) 1658–1663.
[51] H.S. Takhar, A.J. Chamkha, G. Nath, MHD flow over a moving plate in a rotating fluid with magnetic field, Hall currents and free stream velocity, International Journal of Engineering Science 40 (13) (2002) 1511–1527.
[52] A. Wakif, A. Chamkha, I.L. Animasaun, M. Zaydan, H. Waqas, R. Sehaqui, Novel physical insights into the thermodynamic irreversibilities within dissipative EMHD fluid flows past over a moving horizontal riga plate in the coexistence of wall suction and joule heating effects: a comprehensive numerical investigation, Arabian Journal for Science and Engineering 45 (11) (2020) 9423–9438.
[53] E. Magyari, A.J. Chamkha, Combined effect of heat generation or absorption and first-order chemical reaction on micropolar fluid flows over a uniformly stretched permeable surface: The full analytical solution, International Journal of Thermal Sciences 49 (9) (2010) 1821–1828.